Aeroacoustics Conferences
30 May - 1 June, 2016, Lyon, France
22nd AIAA/CEAS Aeroacoustics Conference

Trailing Edge Noise Reduction Using Novel Surface Treatments

Abbas Afshari[1]
Yazd University, Yazd, Iran

Mahdi Azarpeyvand[2]
University of Bristol, Bristol, United Kingdom, BS8 1TR

Ali A. Dehghan[3]
Yazd University, Yazd, Iran

Máté Szőke[4]
University of Bristol, Bristol, United Kingdom, BS8 1TR

A novel trailing edge noise control technique based on upstream manipulation of large coherent turbulent structures using two dimensional surface treatments has been proposed and tested. To demonstrate the capabilities of the proposed trailing edge noise control technique, a long flat-plate model, equipped with several streamwise and spanwise surface pressure microphones, has been designed and built. Flow and noise measurements have been carried out for a variety of surface treatments, with different geometrical patterns and dimensions. The flow behavior downstream of the surface treatment is also studied by employing a single probe hotwire anemometer. Results have shown that the use of such surface treatments can lead to around 8 dB reduction of the surface pressure fluctuations near the trailing edge. More importantly, it has been observed that the spanwise coherence can be significantly reduced over a wide range of frequencies, implying that the large coherent turbulent structures have been successfully removed from the boundary layer. Furthermore, the unsteady surface pressure and boundary layer velocity cross-correlation studies have shown that the correlation between the turbulent structures within the outer region of the boundary layer and the unsteady surface pressure exerted on the surface can be significantly reduced by using treatments with height of only 10% of the boundary layer thickness.

Nomenclature

c	=	flat plate chord, m
d, d^+	=	pinhole diameter, made dimensionless with wall unit
f	=	frequency, Hz
H	=	fence height, mm
p'	=	fluctuating surface pressure, Pa
t	=	trailing edge thickness, m
U_c	=	convection velocity, m/s
u_{rms}	=	root mean square of velocity fluctuations, m/s
U_τ	=	Wall-friction velocity, m/s
U_∞	=	free stream velocity, m/s
x	=	streamwise distance from the flat plate leading edge, m

[1] School of Mechanical Engineering, Yazd University, PhD student, *afshar.abbas@gmail.com*
[2] Department of Mechanical Engineering, University of Bristol, Senior Lecturer and Royal Academy of Engineering research fellow, *m.azarpeyvand@bristol.ac.uk*
[3] School of Mechanical Engineering, Yazd University, Associate Professor
[4] Department of Mechanical Engineering, University of Bristol, PhD student

ϕ	=	surface pressure power spectral density, Pa^2/Hz
$\Lambda_{p,3}$	=	spanwise length scale, m
δ	=	boundary-layer thickness, m
δ^*	=	boundary-layer displacement thickness, m
Δz	=	spanwise separation between microphones, mm
ε	=	streamwise separation between microphones, mm
γ_p^2	=	coherence of Surface pressure fluctuations
υ	=	kinematic viscosity, m^2/s
τ	=	time delay, s
λ_h	=	convected hydrodynamic wavelength, m
TE	=	trailing edge
PSD	=	Power Spectral Density
SPF	=	Surface pressure fluctuation

I. Introduction

Airfoil self-noise is produced due to interaction of unsteady flow, usually in the form of fluid turbulence, with the surfaces of the airfoil. There are a variety of specific noise generating components associated with airfoil self-noise that are concisely summarized in Ref. [1]. Turbulent boundary layer trailing edge (TBL-TE) broadband noise is one of the airfoil self-noise mechanisms that takes place at high Reynolds numbers when turbulent boundary layers develop over most of the airfoil. As the vortical disturbances in the turbulent boundary layer convect over the trailing edge, they are partially converted into acoustic waves. The physical process of trailing edge noise was described by Roger and Moreau [2] from a point of view of the force balance on the eddies. Over the recent decades, trailing edge noise has received considerable research attention in the form of theoretical, computational and experimental research works. This is due to the importance of the subject in a wide range of applications such as aircraft, underwater vehicles, wind turbines, fans, rotors, propellers, *etc*. [2–5].

Numerous theoretical trailing edge noise models have been developed over the past decades, a summary of which can be found in Ref. [2]. There are two basic approaches for the prediction of far field trailing edge noise: formulations based on the Lighthill [6] acoustic analogy that need hydrodynamic velocity field around the TE, or based on linearized hydroacoustic methods that use the induced hydrodynamic pressure field at some distance upstream of the TE. An example of the first approach is the work of Ffowcs Williams and Hall [7], applied by Wang and Moin [8]. However the determination of the true turbulent source from Lighthill's equation is experimentally difficult, as it requires knowledge of the entire turbulent velocity field as a function of space and time. On the other hand, unsteady surface pressure in the vicinity of the airfoil trailing edge can be easily measured by using flush-mounted unsteady pressure transducers and therefore the majority of noise prediction methods for trailing edge have been formulated based on surface pressure fluctuations, including works done by Chandiramani [9], Chase [10], Amiet [11] and Howe [12]. In this approach, the surface pressure is used as an equivalent acoustic source. According to Amiet's [11] and Howe's [12] formulations, the frequency dependent spanwise length scale of the SPFs, defining the efficiency of scattering at the TE, and convection velocity in the T.E. region are crucial quantities in the determination of the far-field trailing edge noise. Therefore, reducing surface pressure spectra, spanwise turbulent length scale and the eddy convection velocity in the T.E. region will reduce the trailing edge noise.

To reduce the turbulent boundary layer trailing edge noise, various passive airfoil noise control methods have been developed, such as trailing edge serrations [5, 13–25], trailing edge brushes [26-28], porous trailing edge [29-33], airfoil shape optimization [34, 35], trailing edge morphing [36, 37] and recently upstream surface treatment [38]. Sawtooth serrations appeared initially as means to reduce the exhaust noise of a jet engine [39]. Then, it was shown both analytically [13–17] and experimentally [5, 18-25] that trailing edge noise levels can be reduced by modifying the trailing edge geometry by serrations so that flow disturbances are scattered into sound with reduced efficiency. In fact the addition of trailing edge serrations lead to a reduction in the effective spanwise length of the trailing edge. Detrimental effects could occur when serrations were not aligned with the flow [18]. Flexible trailing-edge brushes have demonstrated a significant noise-reduction potential in wind-tunnel tests on flat plates and on a 2-D airfoil. Porous trailing edges can also significantly reduce the sound pressure level at low to mid frequencies. However, an increase in noise at higher frequencies was observed and was attributed to surface roughness effects. While effective, brush and porous edge attachments may have practical limitations, namely the fine pores or spaces between brushes are prone to collect dirt and insects making them ineffective. Airfoil shape optimization such as modification of the thickness or the curve gradient can significantly affect the flow field around the airfoil, leading to improvement in

both the aerodynamic and aeroacoustic performance of the airfoil. Trailing-edge morphing can also effectively reduce the airfoil trailing edge noise over a wide range of flow speeds and angles of attack.

In 2014, Clark *et al*. [40] used a series of canopies, inspired by the owl's downy coating, over the rough surface to suppress roughness noise. All canopies were reported to have a strong influence on the surface pressure spectra, and attenuations of up to 30 dB were observed. This development represented a new passive method for roughness noise control. To investigate the applicability of this method in reducing trailing edge noise, Clark *et al*. [38], in 2015, tested over 20 variants of surface treatments by performing aeroacoustic wind tunnel measurements on a tripped DU96-W180 airfoil. The treatments were installed directly upstream of the trailing edge to modify the boundary layer turbulence prior to interacting by the edge. Compared to the untreated airfoil the treatments were found to be effective, providing broadband attenuation of trailing edge noise of up to 10dB. Furthermore aerodynamic impact of the treatment appeared to be minimal.

Although the effectiveness of upstream surface treatments as a new passive trailing edge noise control method was recently investigated by Clark et al. [38], the mechanisms responsible for the noise control has not been addressed. In the present study, the effects of surface treatments on surface pressure power spectral density, the frequency dependent spanwise length scale and the convection velocity in the T.E. region of a flat plate are investigated. Furthermore, velocity measurements near the trailing edge and the simultaneously measured unsteady velocity and surface pressure data have provided further information about the trailing edge noise reduction mechanisms. The experimental layout is described in section II and the main outcomes of the investigation are presented in section III.

II. Experimental setup

A. Wind tunnel and model

The experiments were carried out in an open subsonic wind tunnel of Yazd University with a test section size of 46 × 46 × 240 cm. Boundary layer correction is achieved by corner fillets extending the length of the contraction cone and the working test section, to ensure a uniform longitudinal pressure in the working section. At the maximum speed of 25 m/s the free stream turbulence intensity has been measured to be less than 0.3%.The wall-pressure fluctuations measurements are often carried out in an acoustically quiet wind tunnel to avoid noise contamination due to the wind tunnel background noise. In the present wind tunnel, the centrifugal forward blades type fan creates low broadband noise.

The flat plate used in the present work has a chord length of 580 mm, a span of 456 mm and a thickness of 8 mm. The leading edge of the model is made to be elliptical with a semi-major axis of 12 mm and a semi-minor axis of 4 mm while the trailing edge is asymmetrically beveled at an angle of 12 ° to cause attached flow on both sides. The model is composed of a main body and a detachable trailing edge part, which allows spanwise microphones to be installed horizontally inside the airfoil trailing edge section. The trailing edge plate is attached to the main body with two side plates. The thickness of the trailing edge is 0.4 mm and therefore the narrowband blunt trailing edge vortex shedding noise is negligible ($t/\delta^* < 0.3$) for all free-stream velocities considered in this study [41]. The experiments were carried out at zero angle of attack and three different free stream velocities, $U_\infty = 10$, 15, and 20 m/s corresponding to Reynolds numbers of $Re_c = 3.87 \times 10^5$, 5.8×10^5, and 7.73×10^5, based on the plate chord length. The blockage ratio of the flat plate model is less than 2 % for all the experiments and hence the wind tunnel walls effects on the measured quantities is negligible [42]. To ensure fully developed turbulent boundary layer, the model was tripped using a rough trip strip which is placed 5 to 10 percent of the cord length downstream of leading edge on upper surface. The detailed CAD view of the flat plate model is shown in Fig. 1.

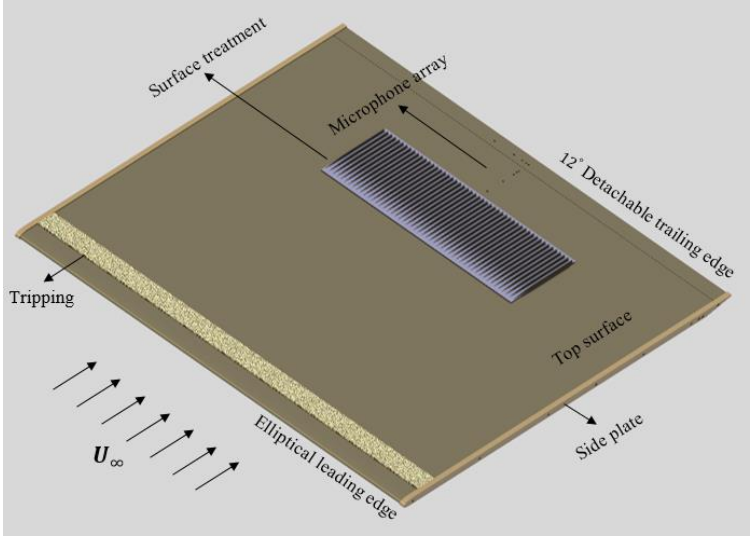

Fig. 1.The flat plate model with a detachable trailing edge, surface treatment and side plates.

B. Instrumentation

The FG-23329-P07 miniature microphones, manufactured by Knowles Acoustics, are employed for unsteady surface pressure measurements. Microphones dimensions are 2.5mm in diameter, 2.5 mm height and with a circular sensing area of 0.8 mm. The same microphones had been used before in other experiments [43, 44] and have shown to be reliable for the frequencies considered in this study. Microphones are embedded in the flat plate under a pinhole mask of 0.4 mm diameter in order to decrease attenuation effects at high frequencies due to the finite size of the microphones sensing area. All pinholes are created with drilling the flat plate surface using an accurate drill machine. Two techniques have been used to embed microphones in the flat plate. At positions far from trailing edge the flat plate is thick enough to embed microphones vertically under the pinhole. Near the trailing edge the microphones have been installed inside the flat plate parallel to the surface (i.e. horizontally). In this arrangement, each microphone was linked to its pin hole on the surface by a horizontal transmission tube. A schematic of both arrangements is depicted in Fig. 2.

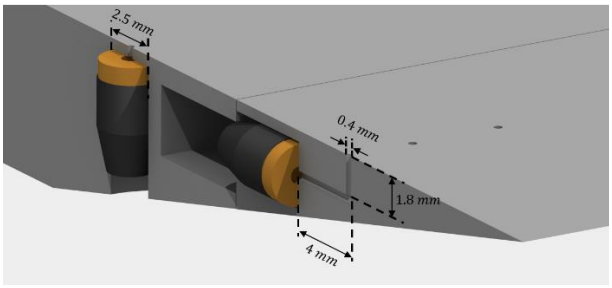

Fig. 2. Illustration of both microphones installation: under pin-hole configuration and with horizontal transmission tube configuration.

Many analytical and experimental investigations were conducted to ensure that the resonant frequencies associated with the selected arrangements shown in Fig. 2 are outside the frequency range of interest. Results showed that the resonant frequencies were greater than 40 kHz and 16 kHz for first and second arrangement, respectively. The frequency response (amplitude and phase) of both arrangements are shown in Fig. 3.

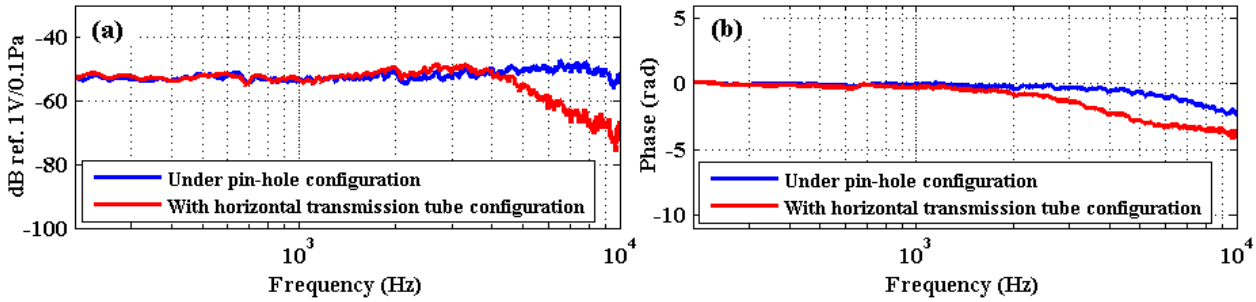

Fig. 3. Frequency response of microphones (a) under pin-hole configuration (microphone No. 7), (b) with horizontal transmission tube configuration (microphone No. 4).

C. Layout of surface microphone array

The Layout of the surface microphone arrays is depicted in Fig. 4. The locations of the pinholes on the upper surface of the flat plate are summarized in Table 1. A total number of 10 microphones are arranged in the form of L-shaped array on the surface of flat plate. A set of microphones are distributed in the streamwise direction from x/c = 0.85 to 0.976 to provide information on the convection velocity of the turbulent eddies. Another set of microphones are distributed along span to measure the spanwise length scale. The space between surface microphones is not equal which leads to a non-redundant population of sensor spacing and maximizing the number of spatial lags available in a cross-correlation comparison.

Many investigations have been carried out to study the important parameters of these arrangements, including the pinhole diameter, the distance of the spanwise microphones from the trailing edge and spanwise spacing of the pinholes [7, 45-52].The finite size of the pressure transducers lead to attenuation of the wall pressure fluctuations spectral levels at high frequencies as reported in references [46-49]. In fact, the pressure measured by transducers of finite size is the average pressure applied across the transducer sensing area and therefore pressure fluctuations smaller than the transducer sensing area are spatially integrated, and thereby attenuated. In order to resolve this issue usually a pinhole mask is used to decrease the effective sensing area of the pressure transducer. On the other hand, Bull and Thomas [50] reported that the discontinuity in the wall due to the presence of a pinhole disturbs the flow and leads to a significant error in the measured wall pressure spectrum at high frequencies. However, the error due to the presence of the pinhole can be eliminated by reducing the pinhole diameter [51, 52]. The ratio of pinhole diameter, d, to the wall unit, v/U_τ ($d^+ = dU_\tau/v$), determines whether or not the attenuation is significant. Schewe [47] concluded that the condition $d^+ < 19$ is sufficient for the proper capturing of all essential wall pressure fluctuations. Gravante *et al.* [48] reported that for the maximum allowable non-dimensional sensing diameter to avoid spectral attenuation at high frequencies is in the range $12 < d^+ < 18$. In the present work, a pinhole mask with a diameter of 0.4 mm is used to reduce spatial averaging. Therefore d^+ is in the range of $12 \leq d^+ \leq 23$ for the free stream velocities, U_∞, ranging from 10 to 20 m/s. Thus, the errors due to the presence of the pinhole and the attenuation effects can be ignored. However, the correction suggested by Corcos [46] has been implemented to the data in order to account for any possible attenuation effects.

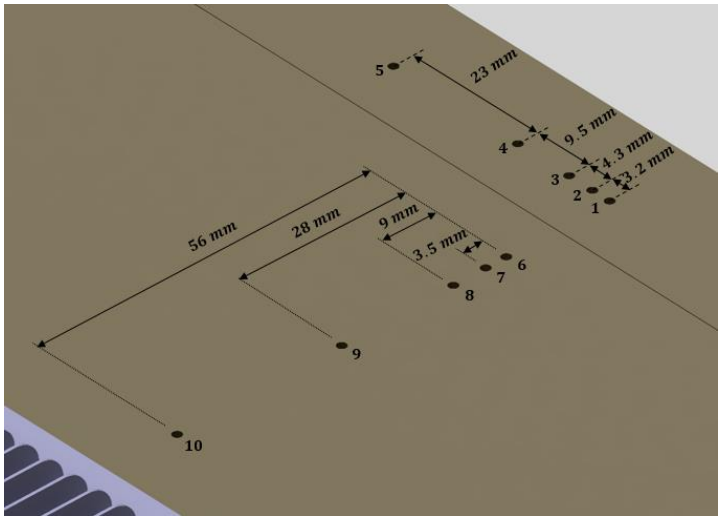

Fig. 4. Map of L-shaped surface microphone array.

Table 1. Position of pressure pinholes in the flat plate.

Microphone number	Distance from T.E. (mm)	Distance from mid span (mm)
1, 2, 3, 4, 5	14.0	0.0, 3.2, 7.5, 17, 40
6,7,8,9,10	31.5, 35, 40.25, 59.5, 87.5	0.0

Special care is taken to select the distance of the spanwise microphones from the trailing edge. This distant must not be so small that the spanwise length scale $\Lambda_{p,3}(\omega)$ and $\phi(\omega)$, which represent the statistics of the incident pressure field, be affected by the scattering process at the trailing edge. On the other hand, it must be near to trailing edge to be representative of the turbulence properties past the trailing edge. Ffowcs-Williams and Hall [7] and Brooks and Hodgson [45] reported that the minimum sensor distance to the TE where scattering effect can be neglected is$\approx \lambda_h/2$, where λ_h is the convected hydrodynamic wavelength of interest ($\lambda_h = U_c/f$). Therefore, due to this criterion and limitation of the minimum thickness at the flat plate TE for microphone installation, the spanwise pinholes are located at 14 mm upstream of the TE (at x/c = 0.976). Therefore, it can be concluded that the measured surface pressure is not contaminated by the scattered pressure field above the 250, 375, and 500 Hz corresponding to the free stream velocities, $U_\infty = 10$, 15, and 20 m/s respectively.

The pinholes in spanwise direction were arranged according to a potential function in order to obtain a good range of distances for all pinhole pairs. The minimum and maximum distance between the pinholes are 3.2 mm and 40 mm. The minimum distance was limited by the microphone dimensions and the maximum distance is selected based on preliminary measurements.

D. Surface treatments

In the present study the blade-shaped fence is chosen as the surface treatment for the flat plate. The design parameters of the fences are illustrated in Fig. 5. The fences were supported by thin substrates glued to the flat plate. The leading and trailing edges of the substrate was faired to the flat plate surface by covering it with 0.1mm thick aluminum tape. The surface treatment is placed on the top surface, upstream of the trailing edge, from about 64% to 82% of the flat plate chord. The profile of the fence leading edge is designed to have the same geometry to that of the turbulent boundary layer shape so that the height of fences, before reaching the maximum height, is proportional to $x^{4/5}$ (x start from fence leading edge). A total number of 9 blade-shaped fences were fabricated using rapid prototyping. The detailed geometry parameters of fences is given in Table 1 in terms of the fence height (H), and spacing (S).

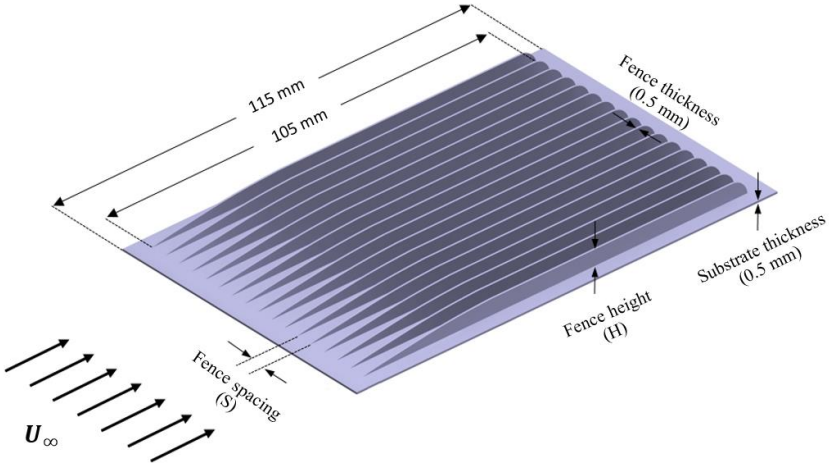

Fig. 5. Blade-shaped fence design parameters.

Table 2. List of surface treatment cases.

Config. No.	1	2	3	4	5	6	7	8	9
Height (mm)	4	4	4	8	8	8	12	12	12
Spacing (mm)	2	4	8	2	4	8	2	4	8

E. Measurement procedure

The unsteady pressure measurements were performed with a total number of 10 FG-23329-P07 miniature microphones. A tube with a length of 110 mm and a diameter of 10 mm along with a high quality loudspeaker were used for the calibration of the microphones. A ¼-inch G.R.A.S. Microphone Type 40BP, calibrated with a G.R.A.S. Sound Calibrator Type 42AB, was used as a reference microphone. Calibration results in the laboratory showed that the sensitivity of the FG-23329-P07 microphones varied approximately between 20 and 24.1 mV/Pa. To provide a transfer function for each microphone, all microphones have been calibrated in-situ with a white noise excitation signal over the frequency range of 200 Hz to 20 kHz. The attenuation and possible resonances induced by the horizontal transmission tubes used to connect the microphones to the pin-holes on the surface are accounted for by this in situ calibration. The method employed in the calibration of the FG-23329-P07 microphones is based on the calibration procedure proposed by Mish [53]. The microphones were powered by a 10-channel power module (manufactured by the Electronics workshop at the Engineering Department of Yazd University) and the data were collected by a 16-channel NI PCI-6023E data acquisition system. The sampling frequency was f_s = 40 kHz, and a total of 800,000 samples were recorded over 20 s. The spectral analysis of the recorded data is done by using the power spectral density (PSD) function of pwelch in MATLAB with a Hamming window function, 50% overlap and a reference pressure of 2×10^{-5} Pa. Reliable and repeatable measurements are achieved for all microphones.

In order to better understand the flow structure and the energy content of the turbulence structures, several velocity measurements have been performed in the boundary layer and in the wake of the trailing edge using a single constant temperature hot-wire anemometer. The sensing element of probe is a standard 5μm diameter tungsten wire with a length of 1.25 mm. The probe was calibrated both statically and dynamically by a standard Pitot tube and a square wave test procedure and all data are low-pass filtered with a suitable cut-off frequency. The probe is traversed in the boundary layer or in the wake by using a three axis traverse unit controlled by stepper motors with 0.01 mm accuracy. The traverse unit allowed continuous movement in the streamwise (x), spanwise (z) and vertical (y) directions. The data were recorded at a sampling frequency of 40 kHz for a sampling time of 10 s.

III. Results and Discussion

Measurements were carried out at zero angle of attack for three different freestream velocities, $U_\infty = 10$, 15, and 20 m/s, corresponding to chord Reynolds numbers of $Re_c = 3.87 \times 10^5$, 5.8×10^5, and 7.73×10^5 respectively. Since measurements at all flow speeds follow the same trend, only the results for U_∞=10 m/s is presented here. For all cases the flat plate boundary layers were fully turbulent, having been tripped as described in section II.A. For all test cases mentioned in Table 2, unsteady surface pressure and hotwire measurements were made simultaneously.

As the turbulent flow field around the trailing edge is the source of trailing edge noise, velocity measurements near the trailing edge of the flat plate with and without surface treatments (baseline) are studied to gain insight into the mechanism by which fences affect flow structure. Figure 6 shows the variation in boundary layer mean velocity profile (u/U_∞) and turbulent intensity profile ($u_{\mathrm{rms}}/U_\infty$) measured for the Baseline and treated flat plate at the position of microphone No. 4 (x/c = 0.976). As shown in this figure, the mean velocity profiles for all surface treatments differ significantly, indicating that the fences alter the downstream flow structures, especially near the wall. Mean velocity reduction is observed for all surface treatments compared to the baseline flat plate. Also, it can be observed that the maximum amplitude of the turbulent intensity for all surface treatment are significantly larger than the baseline, *i.e.* up to 25% increase for Config. 7 (H=12, S=2) and it occurs at about $y/\delta = 0.25$. However, the turbulent intensity in the vicinity of the wall and also far away from the wall decreases as a result of the fence presence. Variations in the boundary layer mean velocity and turbulent intensity profile increases with increasing the fences height or decreasing the space between fences.

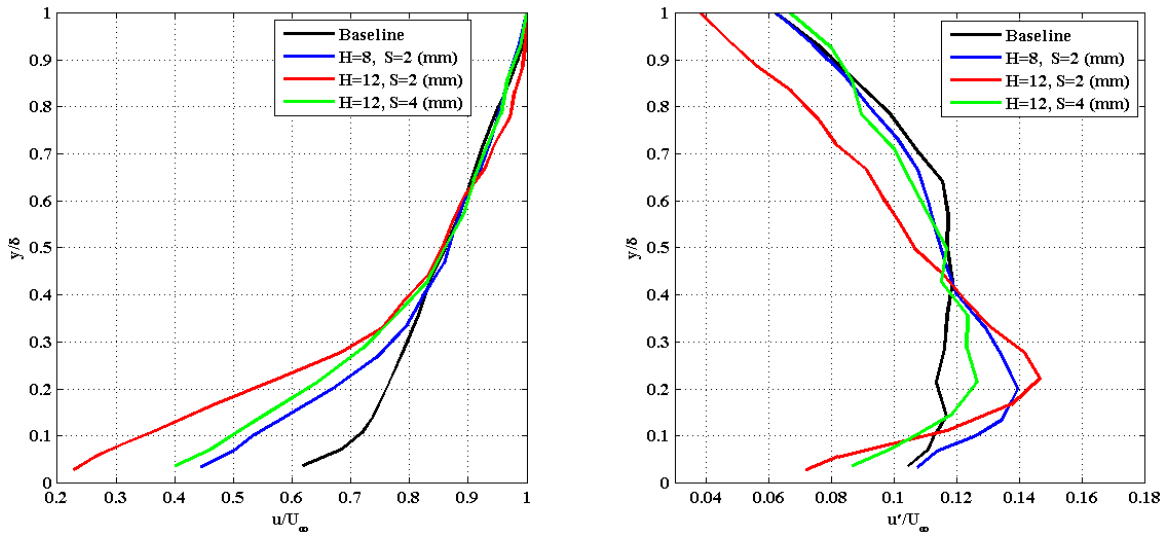

Figure 6. Boundary layer mean velocity and turbulence intensity profiles at the position of microphone No. 4 (x/c = 0.976) at U_∞=10 m/s. *Showing the effects of fence height on Boundary layer mean velocity and turbulence intensity profiles compared to the Baseline.*

The turbulence energy content of the flow structures within the boundary layer of the flat plate, with and without surface treatment, has also been studied. The velocity power spectral density (PSD) results have been measured at 14 mm (x/c=0.976) upstream of the trailing edge *i.e.* the position of spanwise microphones. Results are presented in Figs. 7 and 8 which demonstrate the PSD contour plots for treated flat plate, normalized with the results from the untreated airfoil (baseline) ($\Delta PSD = 10log_{10}(\Phi_{uu,treated}/\Phi_{uu,Baseline})$). It can be observed that surface treatment can lead to an increase in the energy content of the turbulent structure in the buffer region for all frequencies. However, in the areas near the wall and for some cases far away from the wall the energy content of the turbulent structure decreases compared to the baseline case. The region of the velocity power spectral density reduction near the wall increases at higher frequencies. Furthermore, results show that the reduction of the energy content of the turbulent structures near the wall increases with increasing the fence height and spacing.

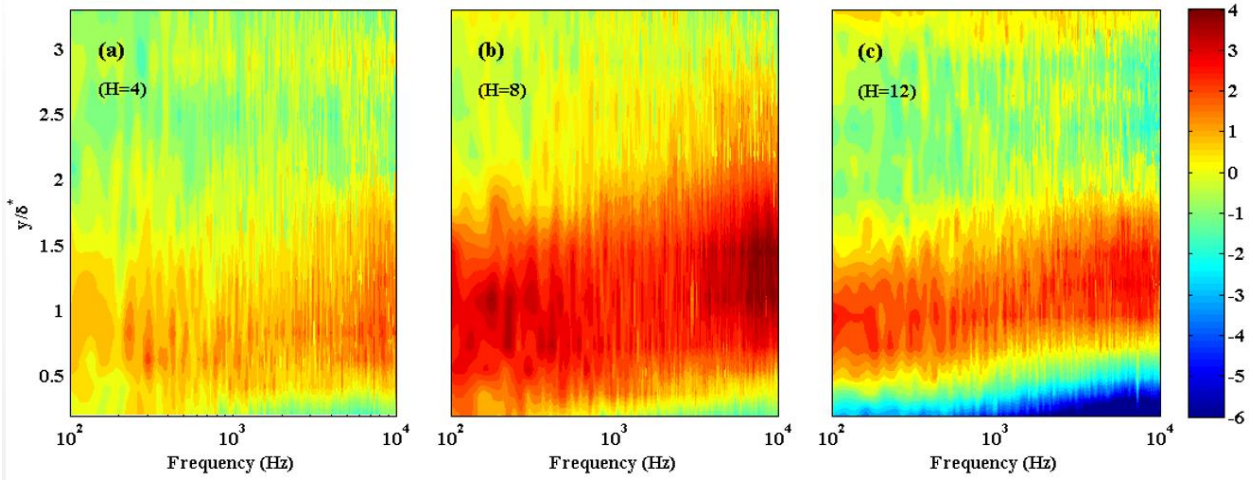

Figure 7. Normalized velocity power spectral density (PSD) contour plots of treated flat plate normalized with Baseline at 14 mm (x/c=0.976) upstream of the trailing edge at U_∞=10 m/s. *Showing the effects of fence height on velocity power spectral density compared to the Baseline.*

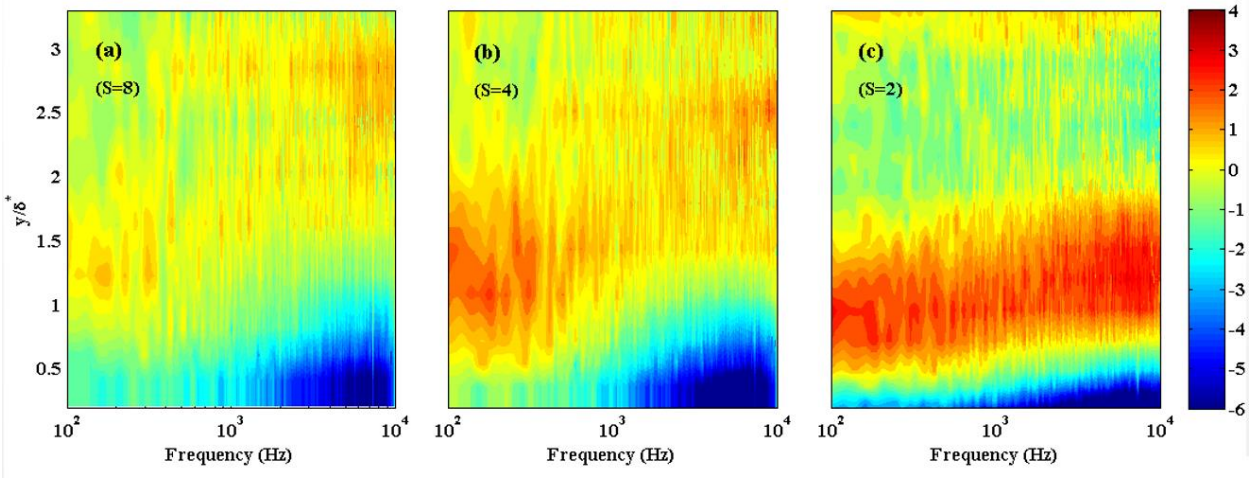

Figure 8. Normalized velocity power spectral density (PSD) contour plots of treated flat plate normalized with Baseline at 14 mm (x/c=0.976) upstream of the trailing edge at U_∞=10 m/s. *Showing the effects of fence spacing on velocity power spectral density compared to the Baseline.*

Figure 9 shows the surface pressure power spectral density measured by microphone No. 4 near the trailing edge of the baseline and treated flat plates (x/c=0.976) referenced to $p_o = 20\ \mu Pa$. The microphone data are corrected based on the calibration procedure and Corcos correction [46] described in section II.C. The wind tunnel background noise power spectral density is also shown in these figures for comparison. The results in Fig. 9 show the effects of the fence height on surface pressure power spectral density compared to the baseline for two fence spacing of 2 and 8 mm. Results show that the surface treatment can increase the surface pressure power spectral density by up to 3.5 dB at low frequencies, but, in the mid and high frequency ranges, a reduction of up to 8 dB is observed. It can be seen that, the efficiency of fences in reducing the surface pressure power spectral density improves with increasing their heights over the entire frequency range of interest. The effect of the fence spacing on the surface pressure power spectral density compared to the baseline for two fence heights of 8 and 12 mm are presented in Fig. 10. Results show that with increasing the spacing between fences, their efficiency in reducing the surface pressure power spectral density is increased.

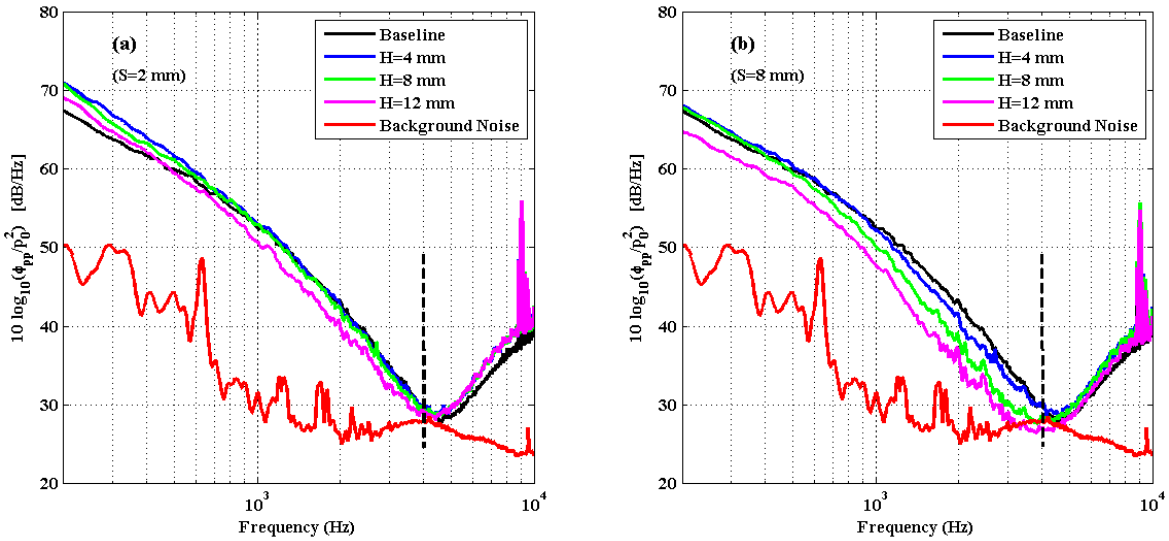

Figure 9. Surface pressure power spectral density referenced to p_o=20 μPa measured by microphone No. 4 on the trailing edge of the tripped flat plate (x/c=0.976) at U_∞=10 m/s. *Showing the effects of fence height on surface pressure power spectral density compared to the Baseline for two fences spacing of 2 and 8 mm.*

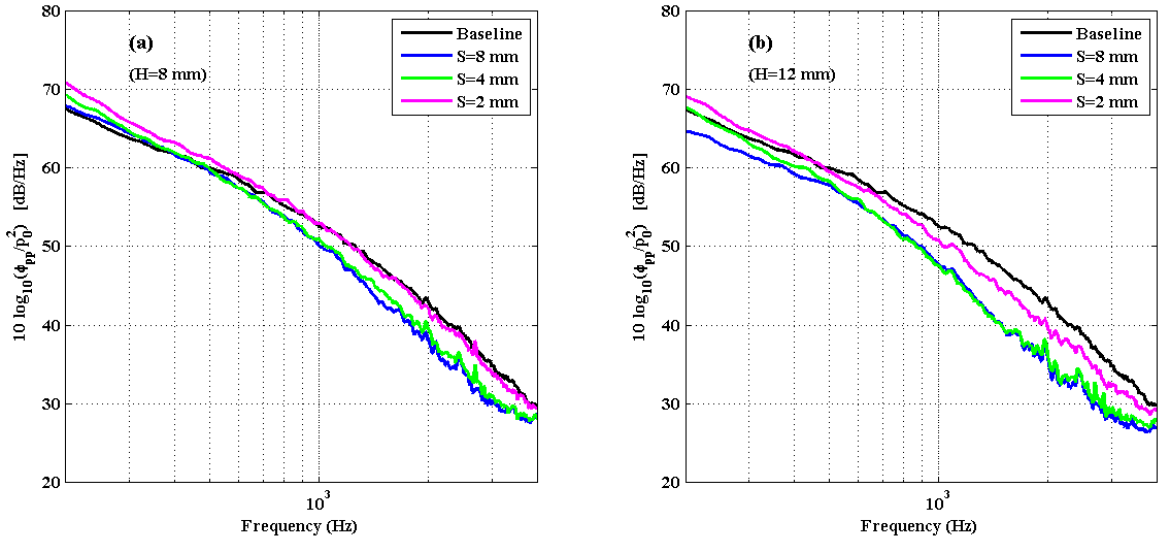

Figure 10. Surface pressure power spectral density referenced to p_o=20 μPa measured by microphone No. 4 on the trailing edge of the tripped flat plate at U_∞=10 m/s. *Showing the effects of fence spacing on surface pressure power spectral density compared to the Baseline for two fences height of 8 and 12 mm.*

As noted in section I, in addition to the trailing edge surface pressure power spectral density, the frequency dependent spanwise length scale of the SPFs and convection velocity in the TE region are also crucial quantities in determining of the far-field trailing edge noise. The lateral coherence measured between the spanwise microphones No. 1 to 5 at x/c=0.976 and different spanwise positions are depicted in Figs. 11 and 12. Results shows that increasing the fence height and decreasing theirs spacing can significantly diminish the lateral coherence between the spanwise microphones in the frequency range between 400 to 1700 Hz. However, the lateral coherence increases at higher frequencies, which require more investigation.

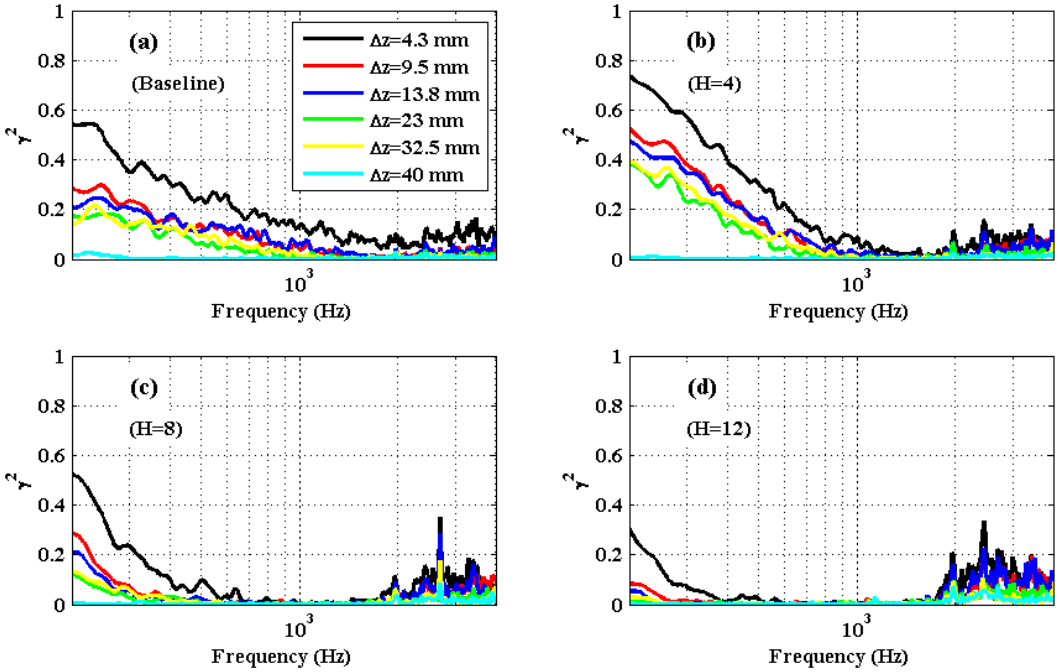

Figure 11. Lateral coherence measured on the tripped Flat Plate between spanwise microphones No. 1 to 5 at x/c=0.976 and different spanwise positions at U_∞=10 m/s. *Showing the effects of fence height on lateral coherence compared to the Baseline (fence spacing=2 mm).*

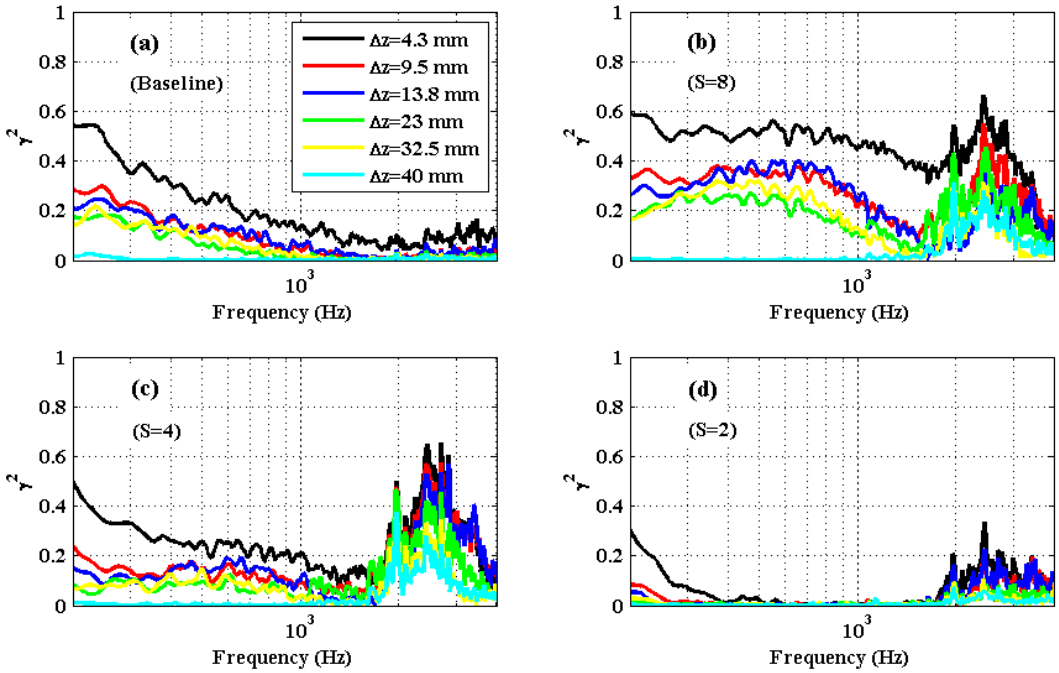

Figure 12. Lateral coherence measured on the tripped Flat Plate between spanwise microphones No. 1 to 5 at x/c=0.976 and different spanwise positions at U_∞=10 m/s. *Showing the effects of fence spacing on lateral coherence compared to the Baseline (fence height=12 mm).*

The spanwise length scale of the surface pressure fluctuations, $\Lambda_{p,3}(\omega)$, was calculated using the frequency dependent spanwise coherence $\gamma^2_{p,ij}(\omega, \Delta z)$ between the spanwise microphones No. 1 to 5 at x/c=0.976 ($\Lambda_{p,3}(\omega) = \int_0^\infty \gamma_{p,ij}(\omega, \Delta z) d\Delta z$). Figure 13 shows the effects of fence height and spacing on spanwise length scale. Results shows that the presence of the fences can significantly reduce the spanwise length scale at low frequencies. However, the surface treatment with large spacing (S) leads to an increase in the spanwise length scale at some frequencies. It is also clear from the results that the spanwise length scale decreases with increasing the fence height and decreasing theirs spacing.

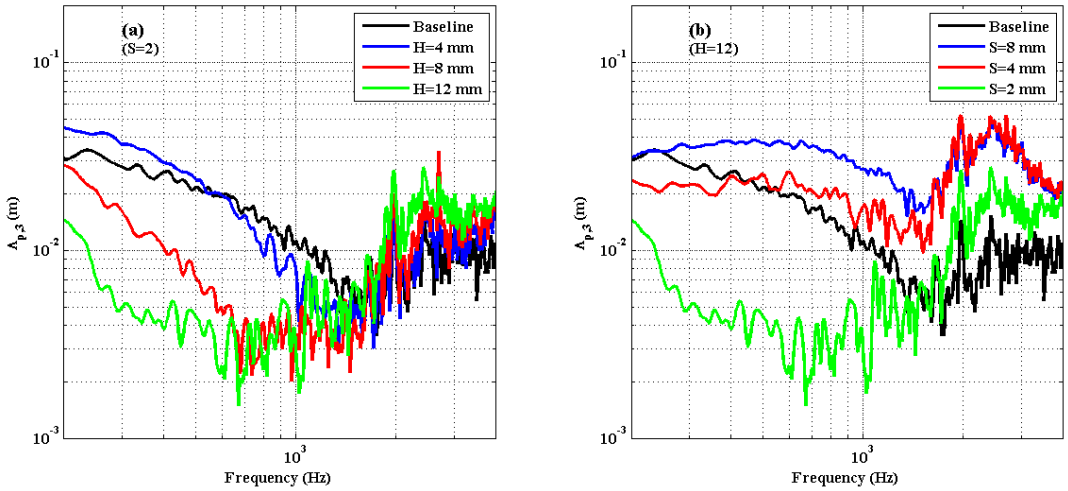

Figure 13. Spanwise length scales. *Showing (a) the effects of fence height (fence spacing=2 mm), (b) the effects of fence spacing (fence height =12 mm) on spanwise length scale. ($\Lambda_{p,3}(\omega) = \int_0^\infty \gamma_{p,ij}(\omega, \Delta z) d\Delta z$).*

The effects of the fence height and spacing on the phase between microphones No. 7 and No. 8 (ε=5.5 mm) near the trailing edge are shown in Fig. 14. The convection velocity can be found using $U_c = 2\pi\Delta f\ \varepsilon\ /\Delta\theta$, where Δf and $\Delta\theta$ are shown in Fig 14. It is clear from the results that the presence of the fences leads to a decrease in Δf and therefore the convection velocity reduction. It is also seen that increasing the fence height and decreasing theirs spacing causes further reduction of the convection velocity. Table 3 summarizes the values of the convection velocity of the turbulent eddies in the boundary layer estimated by phase between microphone No. 7 and No. 8 (ε=5.5 mm) near the trailing edge for the baseline and some treated cases. As seen, the surface treatments lead to a reduction of up to 30 %.

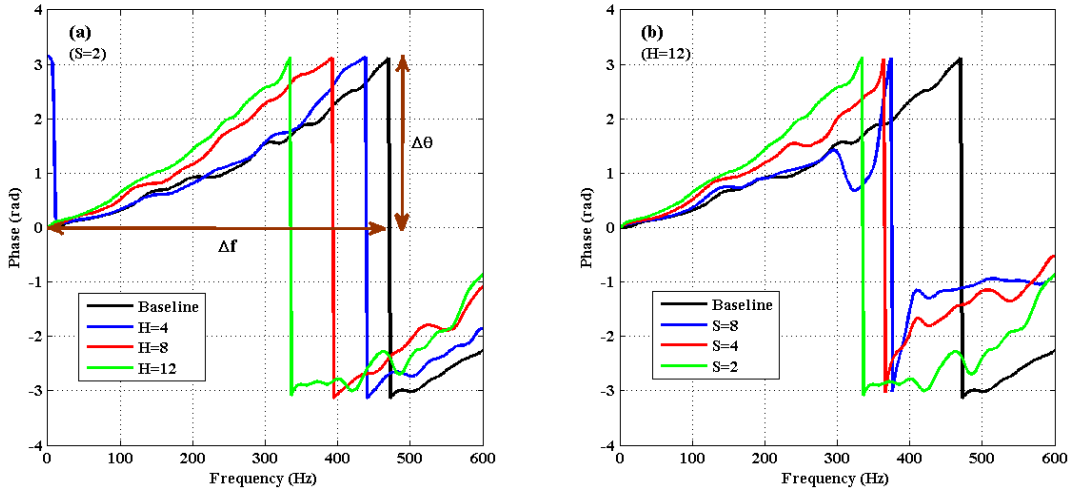

Figure 14. Phase between microphone No. 7 and microphone No. 8 (ε=5.5 mm). *Showing (a) the effects of fence height (fence spacing=2 mm), (b) the effects of fence spacing (fence height =12 mm) on convection velocity ($U_c = 2\pi\Delta f\varepsilon/\Delta\theta$) compared to the Baseline.*

Table 3. Convection velocities calculated from the phase between microphone No. 7 and No. 8 (ε=5.5 mm)

Configuration	Baseline	(H=4, S=2)	(H=8, S=2)	(H=12, S=2)	(H=12, S=8)	(H=12, S=4)
U_C/U_∞	0.52	0.48	0.43	0.37	0.4	0.41

To gain better insight into the mechanism by which fences affect the flow structure, the surface pressure and unsteady velocity are simultaneously measured at various locations within the boundary layer above the microphone No. 4 (x/c = 0.976). The temporal cross-correlation coefficient between u′ and p′ can be calculated using $R_{u,p}(\tau, y) = \overline{u'(y, t+\tau)p'(t)}/(U_\infty p_{rms})$, where u′ and p′ are the streamwise velocity and the surface pressure fluctuations, respectively, y is the distance normal to the surface of the flat plate and τ is the time delay between the signals. The contour plots of the temporal cross-correlation coefficient between u′ and p′ are depicted in Figs. 15 and 16. As can be seen, for all cases, the highest correlation occurs in the positive range of the nondimensional time delay $\tau U_e/\delta^*$. This means that the surface pressure fluctuations have highest correlation with the upstream turbulence eddies and therefore the upstream turbulence eddies play the most important role in the generation of the wall pressure fluctuations. It is clear that for the baseline case, the highest correlation occurs nearly at almost entire boundary layer region except the regions very near to the wall. This is an indication of the presence of the large structures with long life spans that maintain their ‘‘coherence’’ over longer distances. In the presence of the fences, results show that the correlation at regions far away from the wall reduces and instead, the correlation at near wall regions increases. Therefore, in the case of treated flat plates, the important mechanism responsible for the wall pressure generation seems to be due to the near wall region structures, where the highest correlation occurs. This is likely to be due to the breaking-up of the large-scale eddies to smaller ones when passing through the fences. These phenomena were found to be consistent with the effects of the fences in reducing the spanwise length scale, as shown in Fig. 13. Furthermore, results show that increasing the fence height and decreasing theirs spacing can improve these beneficial effects.

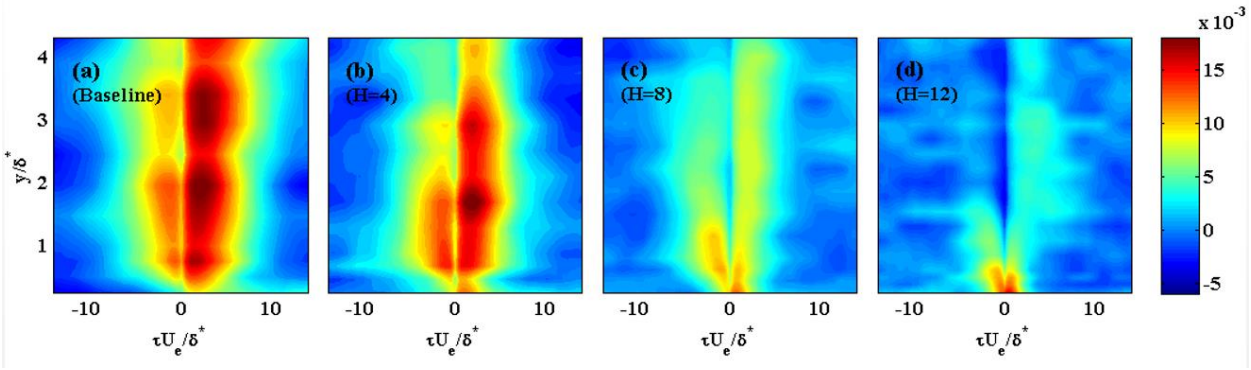

Figure 15. Contour plots of cross correlation coefficient between u′ at 14 mm (x/c=0.976) upstream of the trailing edge, and p′ from microphone No. 4 on the upper surface at U_∞=10 m/s. *Showing the effects of fence height on cross correlation between u′ and p′ compared to the Baseline (fence spacing=2 mm).*

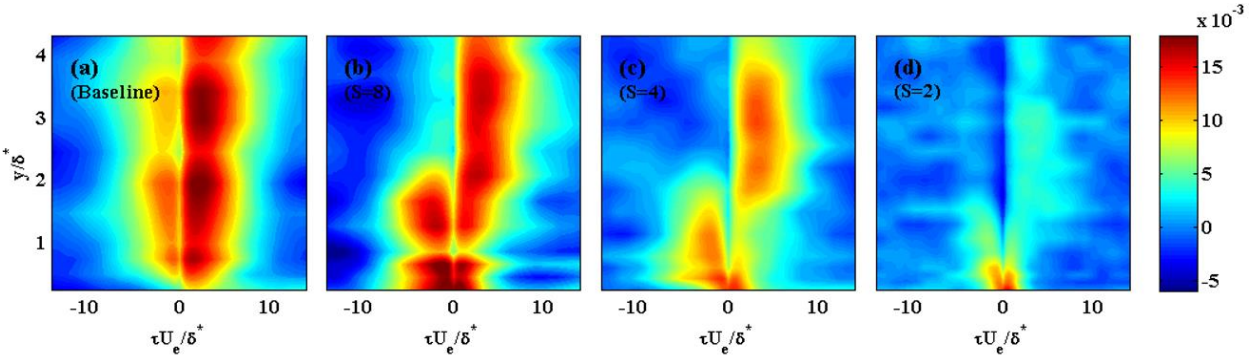

Figure 16. Contour plots of cross correlation coefficient between u′ at 14 mm (x/c=0.976) upstream of the trailing edge, and p′ from microphone No. 4 on the upper surface at U_∞=10 m/s. *Showing the effects of fence spacing on cross correlation between u′ and p′ compared to the Baseline (fence height=12 mm).*

IV. Conclusion

A new trailing edge noise reduction technique based on the use of upstream surface treatments has been proposed and tested. . Results have been provided for various types of surface treatments positioned upstream of the trailing edge of a flat plate. Results revealed that the surface treatment can significantly reduce the surface pressure fluctuations near the trailing edge, lessen the spanwise coherence and spanwise length-scale, and reduce the convection velocity of the turbulent structures. It has also been shown that the cross-correlation between the turbulent structures within the outer region of the boundary layer and the unsteady surface pressure can be significantly reduced.

Acknowledgments

The second author (MA) would like to acknowledge the financial support of the Royal Academy of Engineering.

References

[1]Brooks, T., Pope, S., and Marcolini, M., "Airfoil self-noise and prediction," Tech. rep., NASA Reference Publication 1218, 1989.

[2]Roger, M., Moreau, S., "Trailing Edge Noise Measurements and Prediction for Subsonic Loaded Fan Blades," AIAA Paper No. 2002-2460, 2002.

[3]Blake, W., "Mechanics of Flow Induced Sound and Vibration, Vol. II: Complex flow-structure interactions," Academic Press, New York, 1986.

[4]Lockard, D., and Lilley, G., "The Airframe Noise Reduction Challenge," Tech. Rep. NASA/TM-2004-213013, NASA Langley Research Center, 2004.

[5]Oerlemans, S., Fisher, M., Maeder, T., and Kogler, K., "Reduction of wind turbine noise using optimized airfoils and trailing-edge serrations," AIAA Journal, Vol. 47(6), pp. 1470 – 1481, 2009.

[6]Lighthill, M.J., "On Sound Generated Aerodynamically," I. General Theory, Proceedings of the Royal Society of London. Series A, Mathematical and Physical Sciences, Vol 211, Issue 1107:564–587, 1952.

[7]FfowcsWilliams, J., Hall, L., "Aerodynamic sound generation by turbulent flow in the vicinity of a scattering half-plane," Journal of Fluid Mechanics 40, 657–670, 1970.

[8]Wang, M., Moin, P., "Computation of trailing-edge flow and noise using large-eddy simulation," AIAA Journal 38 (12), 2201, 2000.

[9]Chandiramani, K.L., "Diffraction of evanescent waves with applications to aerodynamically scattered sound and radiation from unbaffled plates," Journal of the Acoustical Society of America, 55:19–29, 1974.

[10]Chase, D.M., "Noise radiated from an edge in turbulent flow," AIAA Journal, 13:1041–1047, 1975.

[11]Amiet, R.K., "Noise due to Turbulent Flow Past a Trailing Edge," Journal of Sound and Vibration, 47:387–393, 1976.

[12]Howe, M.S., "A Review of the Theory of Trailing Edge Noise," Journal of Sound and Vibration, 61:437–465, 1978.

[13]Howe, MS., "Noise Produced by a Sawtooth Trailing Edge," The Journal of Aeroacoustical Sciety of America, 90:482-487, 1991.

[14]Azarpeyvand, M., Gruber, M., Joseph, P. F., "An Analytical Investigation of Trailing-edge Noise Reduction Using Novel Serrations," 19th AIAA/CEAS Aeroacoustics Conference, 2013.

[15]Sinayoko, S., Azarpeyvand, M., and Lyu, B., "Trailing edge noise prediction for rotating serrated blades," 20th AIAA/CEAS Aeroacoustics Conference. 2014.

[16]Lyu, B., Azarpeyvand, M., and Sinayoko, S., "A Trailing-Edge Noise Model for Serrated Edges," 21st AIAA/CEAS Aeroacoustics Conference. 2015.

[17]Lyu, B., Azarpeyvand, M., and Sinayoko, S., "Prediction of noise from serrated trailing edges," Journal of Fluid Mechanics, 793, 556-588, 2016.

[18]Dassen, T., Parchen, R., Bruggeman, J., and Hagg, F., "Results of a wind tunnel study on the reduction of airfoil self-noise by the application of serrated blade trailing edges," European Union Wind Energy Conference and Exhibition Gothenburg, 1996.

[19]Braun, K., van der Borg, N., Dassen, A., Gordner, A., and Parchen, R., "Noise reduction by using serrated trailing edges," European wind energy conference, Dublin, 1997.

[20]Braun, K., Van der Borg, N., Dassen, A., Doorenspleet, F., Gordner, A., Ocker, J., and Parchen, R., "Serrated trailing edge noise," European wind energy conference, Nice, 1999.

[21]Gruber, M., Azarpeyvand, M., and Joseph, P. F., "Airfoil trailing-edge noise reduction by the introduction of sawtooth and slitted trailing-edge geometries," 20th International Congress on Acoustics, Sydney, Australia, 2010.

[22]Gruber, M., Joseph, PF., Azarpeyvand, M., "An Experimental Investigation of Novel Trailing Edge Geometries on Airfoil Trailing Edge Noise Reduction," 19th AIAA/CEAS Aeroacoustic Conference, Berlin, German, 2013.

[23]Moreau D J, Brooks L A , Doolan C J, "On the noise reduction mechanism of a flat plate serrated trailing edge at low-to-moderate Reynolds number," 18th AIAA/CEAS Aeroacoustics Conference, Colorado Springs, CO, AIAA-paper 2012-2186.

[24]Moreau, D. J., and Con J. D., "Noise-reduction mechanism of a flat-plate serrated trailing-edge," AIAA journal, Vol. 51, No. 10, pp. 2513– 2522, 2013.

[25]Xiao, L., Azarpeyvand, M., and Theunissen, R., "Aerodynamic and Aeroacoustic Performance of Serrated Airfoils," 21st AIAA/CEAS Aeroacoustics Conference. 2015.
[26]Herr, M., Dobrzynski, W., "Experimental Investigations in Low Noise Trailing-Edge Design," AIAA Journal, 43(6), 1167-1175, 2005.
[27]Herr, M., "Experimental Study on Noise Reduction through Trailing Edge Brushes," New Results in Numerical and Experimental Fluid Mechanics V, 2006.
[28]Finez, A., Jondeau, E., Roger, M., Jacob, M.C., "Broadband noise reduction with trailing edge brushes," 16th AIAA/CEAS Aeroacoustics Conference, Stockholm, Sweden, AIAA-paper 2010-3980.
[29]Bohn, A. J., "Edge noise attenuation by porous-edge extensions," AIAA Paper 1976-0080.
[30]Howe, MS., "On the Added Mass of a Perforated Shell, with Application to the Generation of Aerodynamic Sound by a Perforated Trailing Edge," Proceedings of the Royal Society A: Mathematical, Physical and Engineering Science, 365(1721), 209-233, 1979.
[31]Fink, M. R., "Model tests of airframe noise reduction concepts," AIAA Paper 1980-0979.
[32]Geyer, T., Sarradj, E., Fritzsche, C., "Measurements of the Noise Generation at the Trailing Edge of Porous Airfoils," Experiments in Fluids, 48(2), 291-308, 2010.
[33]Geyer, T., Sarradj, E., "Trailing edge noise of partially porous airfoils," 20th AIAA/CEAS Aeroacoustics Conference, Atlanta, GA, 2014.
[34]Jones, BR., Crossley, WA., Lyrintzis, AS., "Aerodynamic and Aeroacoustic Optimization of Rotorcraft Airfoils via a Parallel Genetic Algorithms," Journal of Aircraft, 37(6), 1088-1096, 2000.
[35]Gocmen, T., Ozerdem, B, "Airfoil Optimization for Noise Emission Problem and Aerodynamic Performance Criterion on Small Scale Wind Turbines," Energy, 41, 62-71, 2012.
[36]Ai, Q., Azarpeyvand, M., Lachenal, X., and Weaver, PM., "Aerodynamic and aeroacoustic performance of airfoils with morphing structures," Wind Energy, 2015.
[37]Ai, Q., Kamliya Jawahar, H., and Azarpeyvand, M., "Experimental investigation of aerodynamic performance of airfoils fitted with morphing trailing edges," 54th AIAA Aerospace Sciences Meeting, 2016.
[38]Clark, I. A., Alexander, W. N., Devenport, W. J., Glegg, S., Jaworski, J. W. and Daly, C., "Bio-Inspired Trailing Edge Noise Control," 21th AIAA/CEAS Aeroacoustics Conference, Dallas, TX, 22-26 June 2015.
[39]Ver, I. L. "Noise of jet engine test cells," Jet Engine Test Cell Meeting, Naval Facilities Engineering Command, Alexandria, 1987.
[40]Clark, I. A., Devenport, W. J., Jaworski, J. W., Daly, C., Peake, N. and Glegg, S., "The Noise Generating and Suppressing Characteristics of Bio-Inspired Rough Surfaces," AIAA/CEAS 20th Aeroacoustics Conference, Atlanta, GA, 16-20th June. AIAA paper 2014-2911.
[41]Blake, W., "Mechanics of Flow-Induced Sound and Vibration," Applied Mathematics and Mechanics, Vol. 17, 1986.
[42]Barlow, J.B., Rae, W.H, Pope, A., "Low-Speed Wind Tunnel Testing," 3rd edn. Wiley, New York, 1999.
[43]Garcia-Sagrado, A., Hynes, T., "Wall pressure sources near an airfoil trailing edge under separated laminar boundary layers," AIAA Journal 49 (9), 2011.
[44]Gruber, M., "Airfoil noise reduction by edge treatments," Doctoral Thesis, University of Southampton, Faculty of Engineering and the Environment, 2012.
[45]Brooks, T. F. and Hodgson, T., "Trailing Edge Noise Predictions from Measured Surface Pressures," Journal of Sound and Vibration, 78:69–117, 1981.
[46]Corcos, G.M., "Resolution of pressure in turbulence," Journal of the Acoustical Society of America 35 (2), 1963.
[47]Schewe, G., "On the structure and resolution of wall-pressure fluctuations associated with turbulent boundary-layer flow," Journal of Fluid Mechanics, 134, 311–328, 1983.
[48]Gravante, S.P., Naguib, A.M., Wark, C.E., Nagib, H.M., "Characterization of the pressure fluctuations under a fully developed turbulent boundary layer," AIAA Journal 36 (10), 1998.
[49]Goody, M., "Empirical spectral model of surface pressure fluctuations," AIAA Journal 42 (9), 2004.
[50]Bull, M. K., and Thomas, A. S. W., "High Frequency Wall-Pressure Fluctuations in Turbulent Boundary Layers," The Physics of Fluids, Vol. 19, No. 4, pp. 597-599, 1976.
[51]Bull, M. K., "Wall Pressure Fluctuations beneath Turbulent Boundary Layers: Some Reflections on Forty Years of Research," Journal of Sound and Vibration, Vol. 190, No. 3, pp. 299-315, 1996.
[52]Goody, M., "An Experimental Investigation of Pressure Fluctuations in Three-Dimensional Turbulent Boundary Layers," Ph.D. Dissertation, Aerospace Engineering, Virginia Polytechnic Institute and State University, 1999.
[53]Mish, P., "Mean Loading and Turbulence Scale Effects on the Surface Pressure Fluctuations Occurring on a NACA0015 Airfoil Immersed in Grid Generated Turbulence," M.S. Thesis, Virginia Polytechnic Inst. and State Univ., Blacksburg, VA, 2001.